Research and Application of Array Dielectric Logging Tool

Zhiqiang Li*, Xinghai Gui, Zhiqiang Yang, Chen Li, Junyi Li and Yongli Ji
The 22nd Research Institute of China Electronics Technology Group Corporation.
Email:lizhiqiang316@126.com

Keywords: Array dielectric logging tool, lateral wave, finite-element, detecting depth, vertical resolution, thin interbed layer

Abstract: Dielectric logging is an important tool in geophysical exploration. For formation with fresh water and where water salinity is unknown, it has good performance in distinguishing oil and water layers. This paper presents the calculation of electromagnetic field in layered medium by analytical formulas and by finite element method, and compares the accuracy of these two methods. The inversion charts, measurements' depth and vertical resolution are researched. The responses of thin layers and thin interbed layers are also discussed. The designed array dielectric logging tool has been tested in practical wells. Research results show that the analytical formulas are fast and effective for calculating apparatus response of layered medium, and also for retrieving dielectric constant and resistivity. For the array dielectric logging tool, the depth of investigation is 10-25cm, and the vertical resolution is 4cm. The array dielectric logging tool has been tested in XX oil field. For freshwater formation with high resistivity, the measured dielectric constant is about 10 in oil layers, and the measured dielectric constant is about 20 in water layers. The device could distinguish oil and water layers obviously, which offer additional method for formation evaluation.

1 INTRODUCTION

Daev proposed high frequency logging method. The method aimed to measure the phase difference of two receiving coil, under the radiation of electromagnetic wave by transmitting coil. When the working frequency is about several tens of gigahertz, phase difference is mainly due to dielectric constant of rocks. Several Institutes, such as Moscow Institute of Geology, Siberian Branch of the Russian Academy of Sciences and Geophysical Institute, performed a lot of work on high frequency logging. They finished the theoretical research, developed the experimental prototype, and did experiment in wells. The high frequency logging began its commercial production. By then, a new method arose in the field of electric logging, which is measuring the dielectric constant and conductivity of rocks by electromagnetic waves at from several hundreds of kilohertz to several of gigahertz (Hizem et al., 2008; Freedman and Grove, 1990; Seleznev et al., 2006).

Dunn deduced the formula of lateral wave excited by horizontal electric dipole in three horizontal layers (Dunn, 1986). Wu Xinbao obtained the iterative method of calculating the lateral wave excited by horizontal magnetic dipole in two horizontal layers (Wu and Pan, 1992; Wu and Pan, 1990). Chew proposed numerical model-matching method(NMM) in calculating the response of vertical magnetic dipole in cylindrical layers (Chew and Gianzero, 1981). Liu Manfen deduced the formula of the response of arbitrary oriented dipole in dielectric media (Liu et al., 1994).

2 FORMULAS OF LATERAL WAVES IN LAYERED MEDIA

2.1 Electromagnetic Fields in Spherical Coordinates within Homogenous Media

The electromagnetic fields within homogenous media are

$$E_\varphi = -\frac{i\omega\mu r e^{-jkL}(1+ikL)}{4\pi L^3} \quad (1)$$

$$H_z = -\frac{M e^{-jkL}(1+ikL)}{2\pi L^3} \quad (2)$$

in which, ω is angular frequency, μ is magnetic permeability, r is the radius of receiving coil, L is the distance between transmitting point to receiving point, M is the magnetic dipole moment of transmitting coil. $k = \sqrt{-i\omega\mu(\sigma + i\omega\varepsilon)}$ is wave

Li, Z., Gui, X., Yang, Z., Li, C., Li, J. and Ji, Y.
Research and Application of Array Dielectric Logging Tool.
In *Proceedings of the International Workshop on Environment and Geoscience (IWEG 2018)*, pages 406-414
ISBN: 978-989-758-342-1

number, where σ is electrical conductivity of formation, ε is dielectric constant of formation.

2.2 Formulas of Lateral Waves in Horizontally Layered Media

According to the former research results, the size, curvity and electrical conductivity of probe plate could be omitted. So the transmitting antenna could be equivalent to magnetic dipole. The problem is reduced to electromagnetic field excited by magnetic dipole in horizontally layered media.

As in Figure 2, region 1 is mud cake, region 2 is flushed zone, region 3 is undisturbed zone, in which the wave numbers respectively are $k_1 = \omega\sqrt{\mu_1\tilde{\varepsilon}_1}$, $k_2 = \omega\sqrt{\mu_2\tilde{\varepsilon}_2}$, and $k_3 = \omega\sqrt{\mu_3\tilde{\varepsilon}_3}$, in which ω is angular frequency, μ_1, μ_2 and μ_3 are the magnetic permeability in region 1, region 2 and region 3, and $\tilde{\varepsilon}_1$, $\tilde{\varepsilon}_2$ and $\tilde{\varepsilon}_3$ are the complex dielectric constants in region 1, region 2 and region 3. The horizontal magnetic dipole is at the origin point, in the direction of *x*, and with magnetic dipole moment of M, See Figure 1.

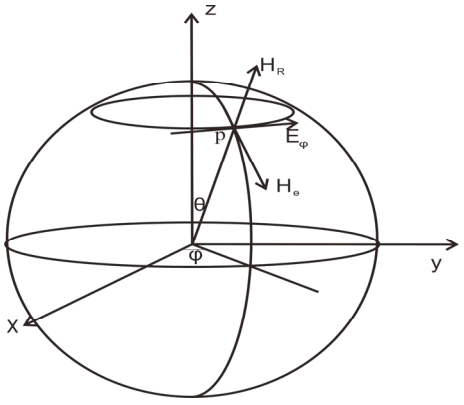

Figure 1: Magnetic dipole in spherical coordinates.

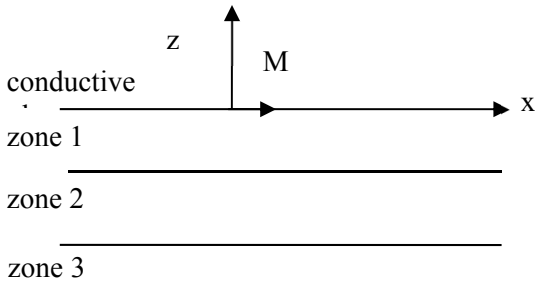

Figure 2: Model of dielectric logging.

From Maxwell's equations, we know:

$$\begin{cases} \nabla \times \vec{E}_i = i\omega\vec{B}_i + i\omega\mu_0\vec{M}_i^0 \\ \nabla \times \vec{B}_i = -i\omega\mu_0\bar{\varepsilon}_i\vec{E}_i \\ \nabla \cdot \vec{E}_i = 0 \\ \nabla \cdot \vec{B}_i = -\mu_0\nabla \cdot \vec{M}_i^0 \end{cases} \quad (3)$$

in which $\vec{M}_i^0 = \begin{cases} \vec{x}m\delta(x)\delta(y)\delta(z+z_0) & i=1 \\ 0 & i=2,3 \end{cases}$, where *m* is the equivalent magnetic dipole moment of the antenna. In cylindrical coordinate, $\vec{M}_i^0 = \begin{cases} \vec{\rho}\frac{m}{\rho}\delta(x)\delta(y)\delta(z+z_0) & i=1 \\ 0 & i=2,3 \end{cases}$. From Equation 3, we get the expression of z component of electromagnetic field in cylindrical coordinate:

$$\begin{cases} (\nabla^2 + k_1^2)E_{1z} = -\dfrac{-i\omega\mu_0 m}{\rho^2}\dfrac{d}{d\varphi}\delta(\varphi)\delta(z+z_0) \\ (\nabla^2 + k_1^2)E_{2z} = 0 \\ (\nabla^2 + k_1^2)E_{3z} = 0 \end{cases} \quad (4-\text{A})$$

$$\begin{cases} (\nabla^2 + \mathrm{k}_1^2)\mathrm{B}_{1z} = \dfrac{\mu_0 \mathrm{m}}{\rho}\dfrac{\mathrm{d}}{\mathrm{d}\rho}\delta(\rho)\dfrac{\mathrm{d}}{\mathrm{d}\varphi}\delta(\varphi)\delta(\mathrm{z}+\mathrm{z}_0) \\ (\nabla^2 + \mathrm{k}_1^2)\mathrm{B}_{2z} = 0 \\ (\nabla^2 + \mathrm{k}_1^2)\mathrm{B}_{3z} = 0 \end{cases} \quad (4-\text{B})$$

Using Fourier transformation, E_{1z} and B_{1z} are obtained as: $E_{1z} = \frac{\omega\mu_0 m}{2\pi}\sin\varphi\int_0^\infty [\cos\gamma_1 z - P\cos\gamma_1 z]\frac{1}{\gamma_1}J_1(\lambda\rho)\lambda^2 d\lambda$ (5)

$$B_{1z} = \frac{i\mu_0 m}{2\pi}\cos\varphi\int_0^\infty [\sin\gamma_1 z - Q\sin\gamma_1 z]J_1(\lambda\rho)\lambda^2 d\lambda \quad (6)$$

in which,

$$P = \frac{(M+N)e^{ir_1 l_1}}{M\cos(r_1 l_1) + i\sin(r_1 l_1)N}$$

$$Q = \frac{(M'+N')e^{ir_1 l_1}}{M'\sin(r_1 l_1) + i\sin(r_1 l_1)N'}$$

$$M = r_2\bar{\varepsilon}_1\left[(r_3\bar{\varepsilon}_2 - r_2\bar{\varepsilon}_3)e^{ir_2(l_2-l_1)} + (r_3\bar{\varepsilon}_2 + r_2\bar{\varepsilon}_3)e^{-ir_2(l_2-l_1)}\right]$$

$$N = r_1\bar{\varepsilon}_2\left[(r_3\bar{\varepsilon}_2 - r_2\bar{\varepsilon}_3)e^{ir_2(l_2-l_1)} - (r_3\bar{\varepsilon}_2 + r_2\bar{\varepsilon}_3)e^{-ir_2(l_2-l_1)}\right]$$

$$M' = r_2\left[(r_3 - r_2)e^{ir_2(l_2-l_1)} + (r_3 + r_2)e^{-ir_2(l_2-l_1)}\right]$$

$$N' = r_1\left[(r_3 - r_2)e^{ir_2(l_2-l_1)} - (r_3 + r_2)e^{-ir_2(l_2-l_1)}\right]$$

$$r_i = \sqrt{k_i^2 - \lambda^2} \quad (i = 1,2,3)$$

Expand Maxwell's equation shown in Equation 3 into individual components in cylindrical form, and according to Equation 5 and Equation 6, the other components of electromagnetic fields are:

$$B_{1\rho} = \frac{-i\mu_0 m}{2\pi}\cos\varphi\left\{\int_0^\infty\left[-\frac{k_1^2}{2r_1}(J_0(\lambda\rho)+J_2(\lambda\rho)) - \frac{r_1}{2}(J_0(\lambda\rho)-J_2(\lambda\rho))\right]\cos r_1 z\lambda d\lambda + \int_0^\infty\left[\frac{k_1^2 P}{2r_1}(J_0(\lambda\rho)+J_2(\lambda\rho)) + \frac{r_1 Q}{2}(J_0(\lambda\rho)-J_2(\lambda\rho))\right]\cos r_1 z\lambda d\lambda\right\} \quad (7)$$

$$B_{1\varphi} = \frac{i\mu_0 m}{2\pi}\sin\varphi\left\{\int_0^\infty\left[-\frac{k_1^2}{2r_1}(J_0(\lambda\rho)-J_2(\lambda\rho)) - \frac{r_1}{2}(J_0(\lambda\rho)+J_2(\lambda\rho))\right]\cos r_1 z\lambda d\lambda + \int_0^\infty\left[\frac{k_1^2 P}{2r_1}(J_0(\lambda\rho)-J_2(\lambda\rho)) + \frac{r_1 Q}{2}(J_0(\lambda\rho)+J_2(\lambda\rho))\right]\cos r_1 z\lambda d\lambda\right\} \quad (8)$$

$$E_{1\rho} = \frac{-i\omega\mu_0 m}{2\pi}\sin\varphi\left\{\int_0^\infty J_0(\lambda\rho)d\lambda\sin(r_1 z) - \int_0^\infty\left[\frac{P}{2}(J_0(\lambda\rho)-J_2(\lambda\rho)) + \frac{Q}{2}(J_0(\lambda\rho)+J_2(\lambda\rho))\right]\sin r_1 z\lambda d\lambda\right\} \quad (9)$$

$$E_{1\varphi} = \frac{\omega\mu_0 m}{2\pi}\cos\varphi\left\{\int_0^\infty J_0(\lambda\rho)d\lambda\sin(r_1 z) - \int_0^\infty\left[\frac{P}{2}\left(J_0(\lambda\rho)+J_2(\lambda\rho)\right)+\frac{Q}{2}\left(J_0(\lambda\rho)-J_2(\lambda\rho)\right)\right]\sin r_1 z\lambda d\lambda\right\} \quad (10)$$

When $z = 0$,

$$B_{1\rho} = \frac{-i\mu_0 m}{2\pi}\cos\varphi\left\{\int_0^\infty\left[-\frac{k_1^2}{2r_1}\left(J_0(\lambda\rho)+J_2(\lambda\rho)\right)-\frac{r_1}{2}\left(J_0(\lambda\rho)-J_2(\lambda\rho)\right)\right]\lambda d\lambda + \int_0^\infty\left[\frac{k_1^2 P}{2r_1}\left(J_0(\lambda\rho)+J_2(\lambda\rho)\right)+\frac{r_1 Q}{2}\left(J_0(\lambda\rho)-J_2(\lambda\rho)\right)\right]\lambda d\lambda\right\} \quad (11)$$

$$B_{1\varphi} = \frac{i\mu_0 m}{2\pi}\sin\varphi\left\{\int_0^\infty\left[-\frac{k_1^2}{2r_1}\left(J_0(\lambda\rho)-J_2(\lambda\rho)\right)-\frac{r_1}{2}\left(J_0(\lambda\rho)+J_2(\lambda\rho)\right)\right]\lambda d\lambda + \int_0^\infty\left[\frac{k_1^2 P}{2r_1}\left(J_0(\lambda\rho)-J_2(\lambda\rho)\right)+\frac{r_1 Q}{2}\left(J_0(\lambda\rho)+J_2(\lambda\rho)\right)\right]\lambda d\lambda\right\} \quad (12)$$

$$E_{1z} = \frac{\omega\mu_0 m}{2\pi}\sin\varphi\int_0^\infty[1-P]\frac{1}{\gamma_1}J_1(\lambda\rho)\lambda^2 d\lambda \quad (13)$$

in which the ρ component of electromagnetic fields is received by antenna vertical to well axis, and at the same time $\varphi = 0°$. The φ component of electromagnetic fields is received by antenna parallel to well axis, and at the same time $\varphi = 90°$. For the two array antennas, we introduce the amplitude attenuation A(dB) and phase shift $\Delta\varphi$

$$A = 8.686 \times Real\left[ln\frac{H_f}{H_n}\right] \quad (13)$$

$$\Delta\varphi = \frac{180}{\pi} \times Imag\left[ln\frac{H_f}{H_n}\right] \quad (14)$$

2.3 Finite Element Method in Dielectric Media

According to electromagnetic theory and computational electromagnetic, the problem of electric field may come down to the following functional extremum problem (Zhang, 1986; Dhayalan et al., 2018; Chen et al., 2017):

$$J(\vec{E}) = \iiint_\Omega \frac{1}{2\omega^2\mu}\left[k^2\vec{E}\cdot\vec{E} - (\nabla\times\vec{E})^2 + \frac{\vec{J}\cdot\vec{E}}{j\omega}\right]dv \quad (15)$$

$$\nabla\times\vec{E} = i\omega\mu\vec{H} \quad (16)$$

After the discretization of the 3-dimentional formation, stiffness matrix is obtained. Using iterative algorithm, the 3-dimentional response of array dielectric logging tool could be calculated. The detailed content about this could be found in various monographs, so no need to be repeated here.

3 ANALYSIS ON THE CALCULATED RESULTS

3.1 Compare the Calculated Results

Case 1: homogeneous space with dielectric constant of 1, the magnetic permeability of 1, and electrical conductivity from 1e-3S/m to 1S/m. The distance between transmitting and receiving antenna is 0.14m.

Magnetic dipole and Lateral wave are two different analytic methods.

Case 2: homogeneous space with dielectric constant from 10 to 80, the magnetic permeability of 1, and electrical conductivity from 0.1S/m. The distance between transmitting and receiving antenna is 0.14m.

From Table 1 and Table 2, we can see that the results of lateral wave and magnetic dipole is consistent. And under the influence of meshing, the finite element method has an error about 5%.

Table 1: Results in homogeneous formation with different conductivity.

Method		σ s/m		
	1e-3	1e-2	1e-1	1
Hz (Magnetic dipole)	45.5-348.2i	59.4-279.6i	61.3-23.92i	0.123-0.26i
Hz (Lateral wave)	45.1- 348.3i	59.3-279.7i	61.3-23.97i	0.123-0.26i
Hz (Finite element)	46.9-348.7i	59.6-280.0i	61.2-23.6i	0.128-0.26i
Hx (Magnetic dipole)	-455.0+82.6i	-360.4+132.8i	28.03+133.6i	-0.669+1.70i
Hx (Lateral wave)	-455.03+ 82.5i	-360.3+132.7i	28.02+133.6i	-0.669 + 1.70i
Hx (Finite element)	-454.9+82.4i	-360.8+133.0i	28.38+133.8i	-0.628+1.72i

Table 2: Results in homogeneous formation with different dieletric constant.

Method		ε		
	10	30	50	80
Hz (Magnetic dipole)	40.1-478.0i	518.4-1034.6i	1530.4-646.0i	2084.6+894.3i
Hz (Lateral wave)	40.2 - 478.1i	514.1-1036.9i	1533.8- 638.2i	2079.9+908.2i
Hz (Finite element)	39.8- 478.8i	512.2-1037.6i	1535.3- 634.6i	2076.9+914.2i
Hx (Magnetic dipole)	-2184.5+390.1i	-8170.4+4386.1i	-6936.4-1574.2i	11505-27436i
Hx (Lateral wave)	-2185.0+388.8i	-8177.4+4369.3i	-6894.3-15755i	11591-27387i
Hx (Finite element)	-2185.1+386.5i	-8182.8+4353.6i	-6856.9-15767i	11669-27345i

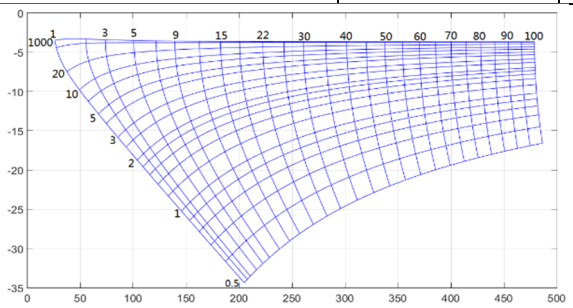

Figure 3a: Inversion chart of vertical polarization.

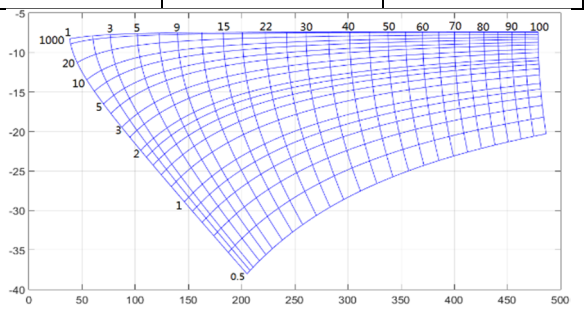

Figure 3b: Inversion chart of horizontal polarization.

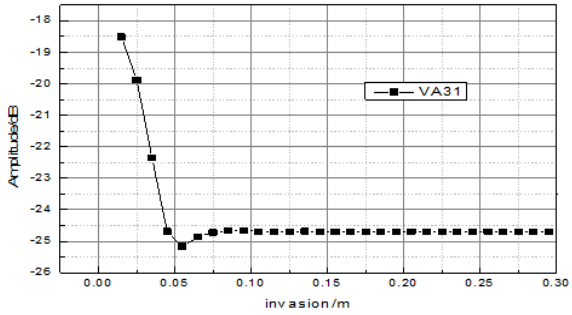

Figure 4a: Amplitude ratio of vertical polarization.

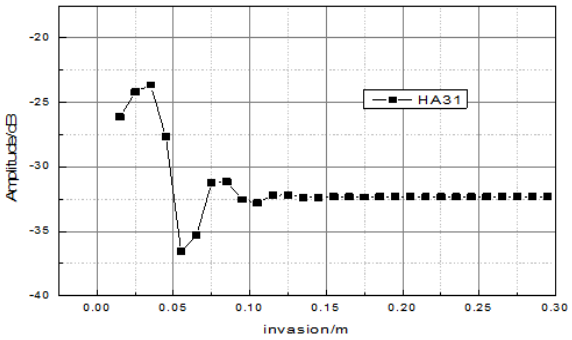

Figure 4b: Amplitude ratio of horizontal polarization.

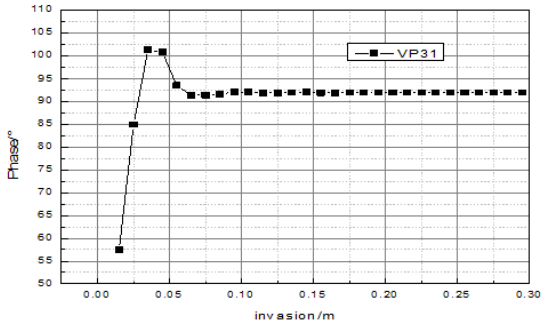

Figure 4c: Phase shift of vertical polarization.

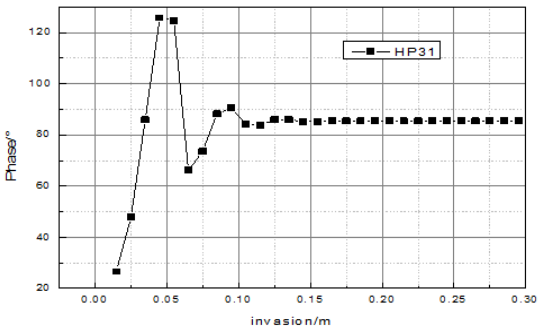

Figure 4d: Phase shift of horizontal polarization.

Figure 4: Detecting depth when resistivity of flushed zone is low.

3.2 Inversion Chart

By calculation, the inversion chart of the two different polarization antenna is obtained as in Figure 3.a and Figure 3.b, in which the lateral axis is phase difference, and the longitude axis is amplitude ratio. The dielectric constant is from 1 to 100, and the electrical resistivity is form 0.5 to 100Ω·m.

3.3 Detecting Depth

Case 1: Mud cake is with thickness of 0.5cm, dielectric constant of 25, conductivity of 1S/m, and flushed zone is with dielectric constant of 20, conductivity of 0.6S/m, and undisturbed zone is with dielectric constant of 15, conductivity of 0.3S/m. Detecting depth is evaluated by the phase difference and amplitude ratio between the nearest and farthest receiving antennas.

Case 2: Mud cake is with thickness of 0.5cm, dielectric constant of 60, conductivity of 0.25 S/m, and flushed zone is with dielectric constant of 12, conductivity of 0.033S/m, and undisturbed zone is with dielectric constant of 9, conductivity of 0.01S/m.

From Figure 4 and Figure 5 it is seen that, in formation with flushed zone of low resistivity, when the radius of flushed zone is larger than 6cm, phase shift and amplitude ratio of vertical polarization do not have obvious changes, which indicate that deeper formation can't be detected. For horizontal polarization, when the radius of flushed zone is larger than 6cm, deeper formation can't be detected. In formation with flushed zone of low resistivity, when the radius of flushed zone is larger than 20cm, phase shift and amplitude ratio of vertical polarization do not have obvious changes, and when the radius of flushed zone is larger than 30cm, phase shift and amplitude ratio of horizontal polarization do not have obvious changes. According to these simulated results, it is seen that detecting depth of horizontal polarization is larger than detecting depth of vertical polarization.

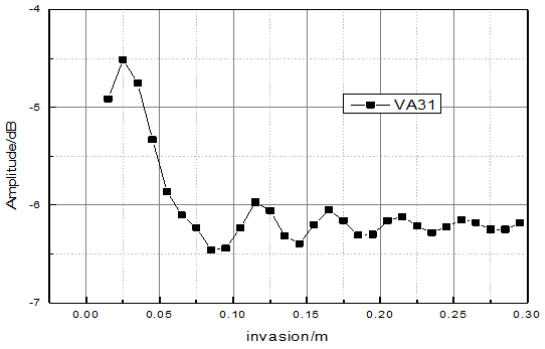

Figure 5a: Amplitude ratio of vertical polarization.

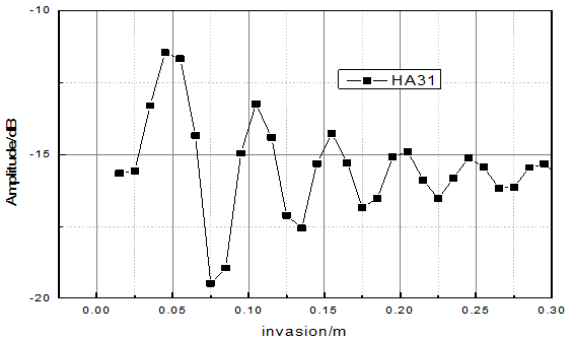

Figure 5b: Amplitude ratio of horizontal polarization.

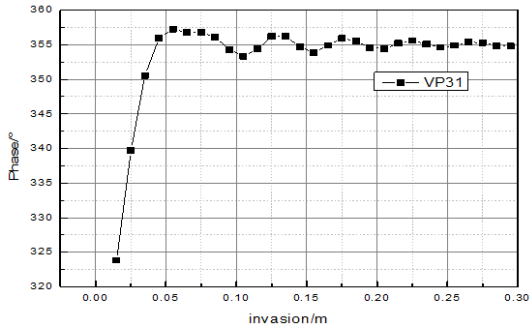

Figure 5c: Phase shift of vertical polarization.

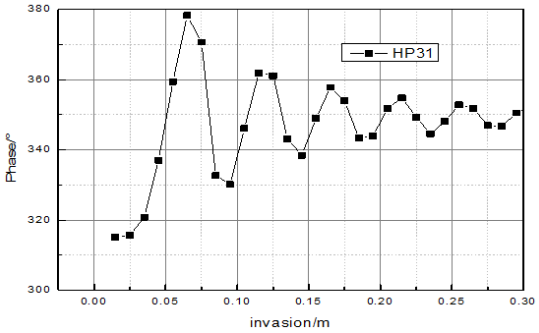

Figure 5d: Phase shift of horizontal polarization.

Figure 5: Detecting depth when resistivity of flushed zone is high.

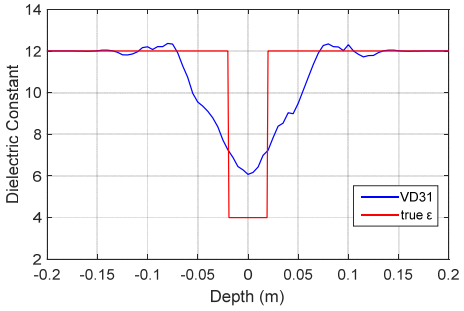

Figure 6a: Dielectric response of vertical polarization.

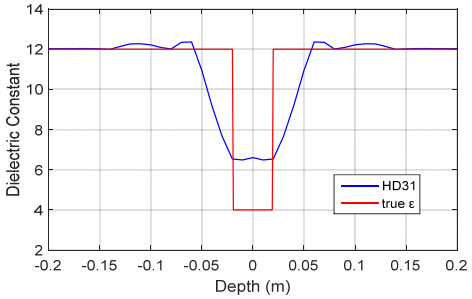

Figure 6b: Dielectric response of horizontal polarization.

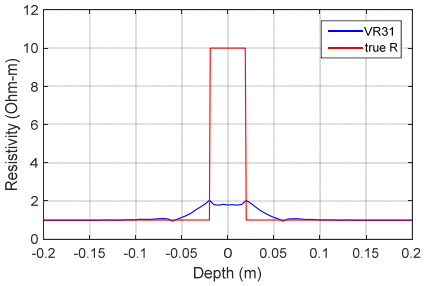

Figure 6c: Resistivity response of vertical polarization.

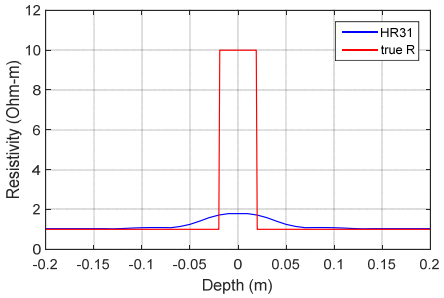

Figure 6d: Resistivity response of horizontal polarization.

3.4 Vertical Resolution

From these response curves as shown in Figure 6, it is seen that in layer with thickness of 4 cm, the apparent dielectric constant is about 6. The array dielectric logging tool is able to distinguish thin layers with thickness of 4 cm, showing the relative high vertical resolution.

4 APPLICATION IN THE PRACTICAL WELLS

Guguba well located at the south rim of Island, with well depth of 2800.80m, and the technical casing is 244.5mm, setting at depth 1945.65m (the Ordovician submarine mountain interface), under which is borehole drilling by 216.0mm drilling bit. Formation of Ordovician and Cambrian is mainly limestone and dolostone. The apertures are well-developed. There are reservoirs of class I, II and III. Porosity distribution is 3-20%. Resistivity of shale is 5-6Ω·m. Resistivity of dense layer is 1000-2000Ω·m. Resistivity of developed apertures is 8-60Ω·m. Abundant logging data is beneficial to evaluate new logging results.

1). From Figure 7 it is seen that, the dielectric curve and resistivity curve show good antisymmetry in dielectric logging data, and agree with the true formation.

2). The dielectric curve and resistivity curve show good response to thin layers and thin interbed layers in dielectric logging data, and are in good agreement with data from micro-scanner logging.

3). From Figure 8 it is seen that,at the depth of 700 m – 710m of XX well, water layer show low resistivity and high dielectric constant.

4). From Figure 8 it is seen that,at the depth of 762.6 m – 774m of XX well, three reservoir layer show slightly high resistivity in conventional logging curves, and are more evaluated as water layers. But in dielectric logging results, the dielectric curves are different in the three reservoir layer, layer 5 and layer 6 should more accurately be evaluated as oil-water layers.

5). Layer 10 and layer 11 in XX well, with resistivity of 10Ω·m, are evaluated as oil according to data of adjacent wells. From dielectric logging results, the dielectric constants are quite low, about 10, which clearly indicate oil layers.

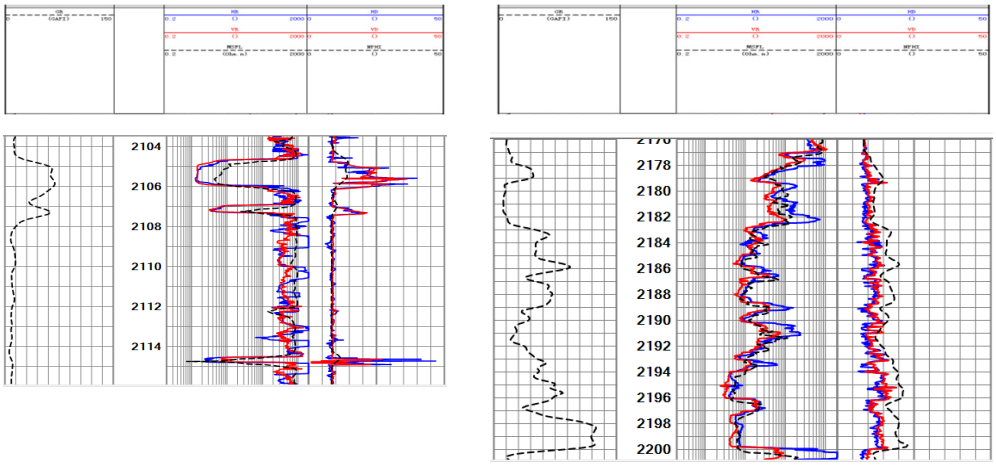

Figure 7a: Comparison between dielectric and resistivity logging data.

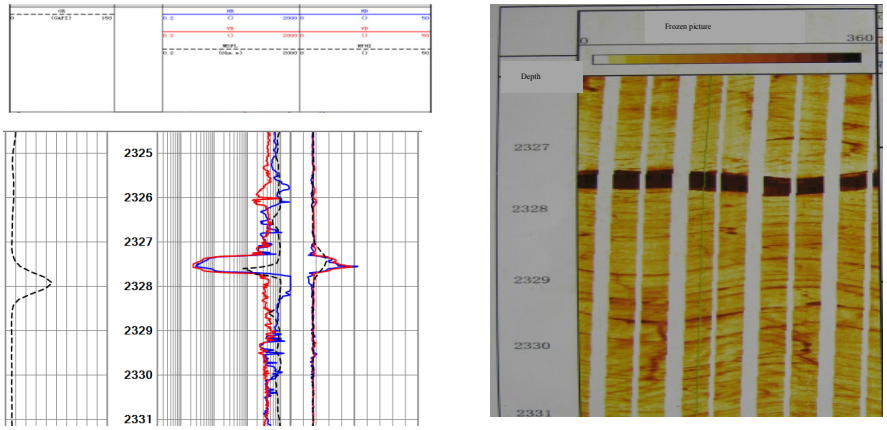

Figure 7b: Comparison between dielectric and micro-scanner logging data in thin layers.

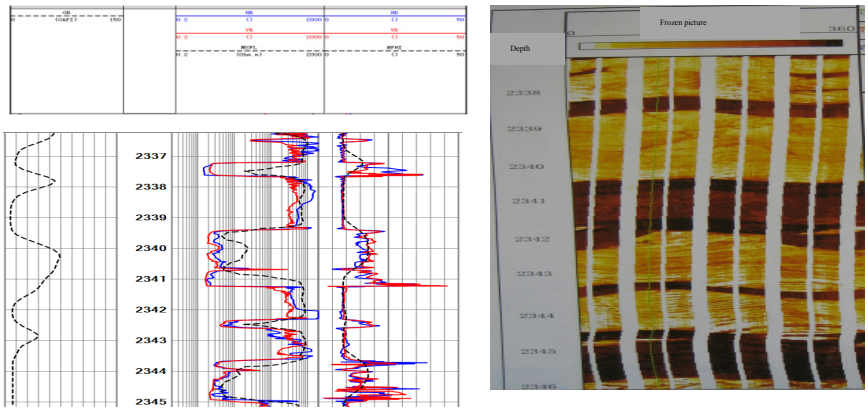

Figure 7c: Comparison between dielectric and micro-scanner data in thin interbed layers.

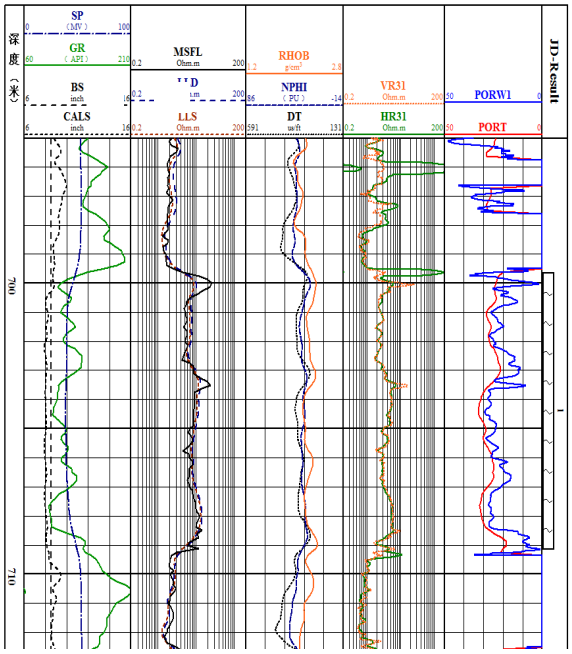

Figure 8a: Dielectric response to water layer in XX well.

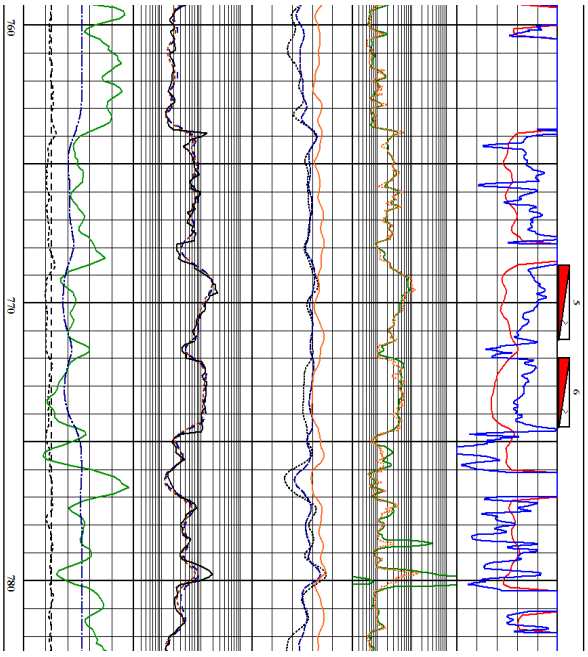

Figure 8b: Dielectric response to oil-water layer in XX well.

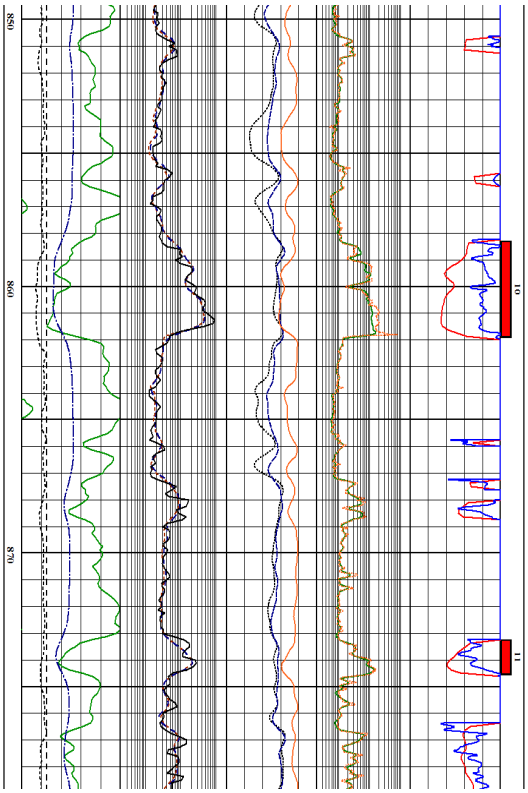

Figure 8c: Dielectric response to oil layer in XX well.

5 CONCLUSIONS

1) Analytical solution is obtained in horizontally layered media, and is compared with homogenous formation. Through three dimensional simulation by finite element method, it is seen that the two methods are reliable and with high accuracy.

2) According to the detecting performance of the dielectric logging tool, vertical resolution is 0.04 m, illustrating that thin layers and thin interbed layers can be effectively distinguished. The detecting depth can reach up to 0.1-0.25 m.

3) Array dielectric logging tool is able to detect resistivity and dielectric constant in both vertical and horizontal direction.

4) In formation with fresh water, resistivity are both high in water layer and oil layer. Using dielectric logging one can make effective evaluation.

REFERENCES

Chen R, Kuang X, Li Z 2017 Numerical computation of infinite Bessel transforms with high frequence *International Journal of Computer Mathematics*

Chew W C and Gianzero S C 1981 Theoretical investigation of the electromagnetic wave propagation tool *IEEE Trans. Geosci. Remote Sens* **19(1)**

Dhayalan R, Kumar A, Rao BP 2018 Numerical analysis of frequency optimization and effect of liquid sodium for ultrasonic high frequency guided wave inspection of core support structure of fast breeder reactor *Annals of Nuclear Energy*

Dunn J M 1986 Lateral wave propagation in a three-layered medium *Radio Science* 21

Freedman R and Grove G P 1990 Interpretation of EPT-G logs in the presence of Mudcake *SPE Formation Evaluation* **5(04)**

Hizem M, Budan H, Deville B, and et al 2008 Dielectric dispersion: A new wire line petrophysical measurement *SPE Annual Technical Conference and Exhibition*

Liu M F, Feng G Q, Wang X J, et a l 1994 Theoretical Investigation of Shoulder Bed Thin Sandwich Effect and Vertical Resolution for The High Frequency Dielectric Logging *Chinese Journal of Geophysics* 37

Seleznev N V, Habashy T M, Boyd A J, et al 2006 Formation properties derived from a multi-frequency dielectric measurement *SPWLA 47th Annual Logging Symposium*

Wu X B and Pan W Y 1990 New Formulas for the Lateral Waves of HMD in a Three-Layered Medium *Chinese Journal of Radio Science* **5(3)**

Wu X B and Pan W Y 1992 The Lateral Wave Propagation in Electromagnetic Wave Propagation Log *Chinese Journal of Geophysics* **35(1)**

Zhang G J 1986 Electrical Logging, PetroIeum Industry Press,